DNMT1-induced miR-133b suppression *via* methylation promotes myocardial fibrosis after myocardial infarction

Songlin Zhang[1], Hang Xie[1], Yajuan Du[1], Boxiang Wang[1], Beidi Lan[1] and Haiyan Wang[1]

[1] *Department of Structural Heart Disease, The First Affiliated Hospital of Xi'an Jiaotong University, Xi'an, China*

Abstract. Myocardial fibrosis is an underlying cause of many cardiovascular diseases. Novel insights into the epigenetic control of myocardial fibrosis are now emerging. The current work is focused on investigating the biological role of DNA methyltransferase 1 (DNMT1) in myocardial fibrosis as well as the underlying mechanism. Our findings revealed that DNMT1 expression levels were upregulated, whereas miR-133b expression levels were decreased in a rat model of myocardial fibrosis following myocardial infarction. *In vitro*, the expression levels of DNMT1 increased and those of miR-133b decreased after Ang-II treatment in cardiac fibroblasts. DNMT1 knockdown inhibited Ang-II-induced cardiac myofibroblast activation, and DNMT1 overexpression increased the proliferation and collagen generation of cardiac myofibroblasts. Furthermore, DNMT1 expression levels decreased, while miR-133b expression levels increased after treatment with 5-Aza (5-Azacytidine, a known inhibitor of DNA methylation) in Ang-II-induced cardiac fibroblasts. BSP (Bisulfite sequencing PCR) results showed a marked decrease in methylation levels in the miR-133b promoter region upon overexpression of DNMT1, whereas knockdown of DNMT1 blocked increased methylation levels in the miR-133b promoter region in Ang-II-induced cardiac fibroblasts. Finally, 5-Aza treatment reduced the progression of myocardial fibrosis after myocardial infarction in rats *in vivo*. Collectively, our results suggest that DNMT1 mediates CTGF expression in cardiac fibroblast activation by regulating the methylation of miR-133b. The present work reveals the unique role of the DNMT1/miR-133b/CTGF axis in myocardial fibrosis, thus suggesting its great therapeutic potential in the treatment of cardiac diseases.

Key words: DNMT1— miR-133b — Methylation — Myocardial fibrosis

Introduction

Cardiac fibrosis is present in a variety of cardiovascular diseases, including myocardial infarction and hypertension. It is characterized by increased abundance of extracellular matrix (ECM) components as well as uneven distribution of these components in cardiomyocytes, and myocardial fibrosis is the main cause of ECM production (Frangogiannis 2021; Liu et al. 2021). Myocardial fibrosis can lead to a variety of cardiovascular diseases, such as arrhythmia, angina pectoris, and cardiac dysfunction, and it is also a predictor of sudden cardiac death (González et al. 2018). Myocardial fibroblasts are the main cells involved in collagen synthesis and account for a very high proportion of cardiac noncardiomyocytes, so during the development of myocardial fibrosis, myocardial fibroblasts are considered to be the main effector cells, and their apoptosis, autophagy, proliferation and activation are important components of myocardial fibrosis (Tallquist 2020; Kurose 2021).

In the context of epigenetics, mechanisms such as DNA methylation, histone modification, and microRNAs (miRs) can also be involved in changes in the biological function of cardiac fibroblasts (Tao et al. 2014; Wo-

Correspondence to: Haiyan Wang, Department of Structural Heart Disease, The First Affiliated Hospital of Xi'an Jiaotong University, 277 West Yanta Road, Xi'an, Shaanxi 710061, China
E-mail: wanghaiyan202012@126.com

jciechowska et al. 2017; Long et al. 2020; Li et al. 2021). DNA methylation is one of the main modes of epigenetic modification and reversibly impacts gene function without changing nucleotide sequences. DNA methyltransferase (DNMT) has a DNA methylation signature that functions to maintain *de novo* methylation and is normally maintained by DNMT1 following DNA replication and cell division, whereas DNMT3A and DNMT3B are mainly involved in promoting *de novo* methylation of previously unmethylated parts of genes (Lyko 2018). In an *in vitro* experiment, DNMT1 was found to maintain the activity of *de novo* methylation of DNMT3 in a murine system, showing that DNMT1 plays an important role in the DNA methylation process and may be associated with epigenetic repair of damaged tissues (Yang et al. 2018). Studies have shown that DNA methylation has an important impact on the progression of fibrosis. Current research on DNMT1 is more focused on liver fibrosis, where it can promote the development of fibrosis, but research on DNMT1 in myocardial fibrosis is rarely reported (Brulport et al. 2020; Zhu et al. 2020).

miRs are small noncoding RNAs that are involved in the posttranscriptional regulation of gene expression, are upstream mediators of multitarget and multigene regulation, and participate in a series of biological processes, such as cell proliferation, differentiation, apoptosis, stress responses and autophagy (Saliminejad et al. 2019; Gierlikowski and Gierlikowska 2022; Zhao et al. 2022). According to relevant reports, miRs are involved in the development of many cardiovascular system diseases and are closely related to the underlying pathological processes (Laggerbauer and Engelhardt 2022). Our previous findings showed that miR-133b could inhibit myocardial fibrosis by targeting connective tissue growth factor (CTGF, also known as CCN2) (Zhang et al. 2021). DNMT1 is not an uncommon subject of mechanistic studies of fibrosis, but its role in myocardial fibrosis has rarely been reported. In this study, we found that DNMT1 expression was significantly upregulated in myocardial fibrosis tissues, which regulated miR-133b expression through methylation and then promoted myocardial fibrosis by targeting CTGF.

Materials and Methods

Animal model

The care and use of male Sprague-Dawley rats weighing 180–230 g were approved by the ethical committee of the First Affiliated Hospital of Xi'an Jiaotong University and adhered to institutional guidelines and ethical standards. Twelve rats were randomly divided into two groups: the Sham group ($n = 6$) and the MI (myocardial infarction) group ($n = 6$). Specific methods were described in previous studies (Zhang et al. 2021).

5-Azacytidine-treatment of a murine model of myocardial fibrosis

Four weeks after model establishment, MI-operated rats were randomly assigned to receive 5-Azacytidine (5-Aza) at a dose of 5 mg/kg or control (DMSO-PBS) *via* intraperitoneal (i.p.) injection ($n = 6$ *per* group). Doses were restarted every 4 days until the end of the study 8 weeks after surgery. Animals were euthanized by exsanguination under 4% isoflurane anesthesia, and their hearts were immediately removed, rinsed in PBS, weighed, and cut in half; the apical side was fixed with 10% formalin (Sigma), and the remaining heart tissue was stored at −80°C until use.

Electrocardiogram test

The BL-420N biological function test system was launched, and the signal input line was connected to BL-420N biological function test system 1 channel. The software was opened, and "circulation test" was selected; then, the "hemodynamics" test item was selected in the submenu. The rats were anesthetized by i.p. administration of 10% chloral hydrate (300 mg/kg), the acupuncture needle was inserted into the subcutaneous tissue of the right front, right hind and left hind limbs of the rat. The acupuncture needle was connected to the signal input line, with the right front limb connected to white, the right hind limb connected to black, and the left hind limb connected to red. At this point, ECG waveforms appeared.

Echocardiographic measurements

Methods were described in previous studies (Zhang et al. 2021).

HE staining

An alcohol gradient was used to dehydrate the tissue. The clearing agent (xylene) was mixed with dehydration solution and paraffin at the same time. The transparent tissue block was successively immersed in 3 cylinders of paraffin (60°C). The embedded paraffin blocks were sectioned using a Leica pathology sample sectioning machine, and the cut tissue sections were placed in a water bath at 40°C for spreading. The anti-detachment slides were tilted and inserted into the water surface to pick up the sections so that the sections were attached to the appropriate position of the slides and baked in a 60°C oven for 3 h. The sections were deparaffinized and then stained with Mayer's hematoxylin staining solution for 5 min, washed and immersed in tap water to restore the blue

color. The sections were then stained with 1% water-soluble eosin staining solution for 5 min, washed, and immersed in tap water for 30 s, 95% alcohol for 30 s, 95% alcohol for 1 min, absolute ethanol I for 5 min, absolute ethanol II for 5 min, xylene I for 5 min, and xylene II for 5 min. After air drying, neutral gum was used for mounting, and the slides were finally examined microscopically. Result interpretation: The nucleus was blue, and the cytoplasm, muscle fibers, collagen fibers and red blood cells were red to varying degrees, which allowed observation of the histomorphological structure.

Masson trichrome staining for collagen

Methods were described in previous studies (Zhang et al. 2021).

Immunohistochemical staining

Dewaxed sections were subjected to antigen retrieval using an electric pottery furnace. The electric pottery furnace was first used to boil the liquid with high-grade heating, and it was then adjusted to the middle grade when the liquid was boiling. At this time, retrieval was started, and the repair time was 15 min. At the appropriate time, the beaker was removed from the microwave oven and placed into cold water for cooling. The slide was removed when the repair solution dropped to room temperature and rinsed with PBS (pH 7.4) 3 times for 3 min each time. Prepared 3% hydrogen peroxide was dropped onto the sectioned tissue, and the sample was incubated at room temperature for 15 min and rinsed three times with PBS for 3 min each time. The slides were dried with absorbent paper, the tissue of the immunized group was circled, and diluted normal goat serum was added dropwise for blocking at room temperature for 30 min to reduce non-specific staining. The excess liquid was shaken off without washing, and then diluted primary antibodies (CTGF 1:100, α-SMA 1:100, DNMT1 1:100, collagen I 1:100) were added dropwise and incubated overnight (15 h) in a humidified box at 4°C after adding the primary antibodies. The sections were rinsed with PBS three times for 3 min each time, and HRP-labeled goat anti-rabbit/mouse secondary antibodies were added dropwise after the sections were dried with absorbent paper and incubated at 37°C for 30 min. The sections were rinsed with PBS 4 times for 3 min each time, the PBS solution was shaken off, the sections were dried with absorbent paper, and freshly prepared DAB chromogenic solution was added dropwise to each section and observed microscopically. The positive signal was brownish-yellow or tan, and color development was terminated by rinsing the sections with tap water at the appropriate time. Mayer's hematoxylin counterstaining was performed at regular intervals for 2 min before restoration of the blue color with PBS buffer. The slides were dehydrated and cleared after being rinsed in water and

finally air-dried in a fume hood. Air-dried sections were observed, and images were acquired under a microscope. Interpretation of results: Blue indicated the nucleus, and brownish-yellow or tan indicated the target protein.

Cardiac fibroblast isolation

Methods were described in previous studies (Zhang et al. 2021).

Cell viability assay

Methods were described in previous studies (Zhang et al. 2021).

Cell transfection

pcDNA3.1/DNMT1 (pcDNA3.1 as control) and si-DNMT1 (siRNA as control) were purchased from Applied Biological Materials (ABM). The miR-133b mimics and control mimics were purchased from RiboBio. Transfections were performed using the Lipofectamine 2000 Kit (Invitrogen) according to the manufacturer's instructions.

Quantitative real-time PCR

Total RNA from tissues and cells was isolated with TRIzol reagent (Invitrogen) according to the manufacturer's instructions. Reverse transcription was performed with the PrimeScript RT Reagent Kit (Takara) according to the manufacturer's protocol. Quantitative real-time PCR was performed using a SYBR Premix Ex Taq™ II Kit (Takara) on a CFX96 real-time PCR system (Bio-Rad) based on the manufacturer's instructions. All assays were performed in triplicate. miR-133b was normalized to small nuclear U6, while the others were normalized to the gene β-actin. The primer sequences are shown in Table 1.

Table 1. Primer sequences for real-time PCR

Genes	Primer sequences (5′–3′)
CTGF	F: AGCAGCGGCATTTGGACAA
	R: CGTGCGAATAGCGACAGTTCT
collagen I	F: GCTTTCAACACGCATG
	R: AACTGCACCTGTACGATCG
DNMT1	F: CGCTCATTGGCTTTTCTACCG
	R: AGAACTCGACCACAATCTT
α-SMA	F: CAGAGGGAAGAGTTCAG
	R: CTTGGTCTGGAGGAGACCT
β-actin	F: TCCCTGGAGAAGAGCTACGA
	R: AGCACTGTGTTGGCGTACAG

F, forward; R, reverse.

Western blotting

Protein extraction of cardiac fibroblasts: Cells requiring treatment were removed, washed twice with PBS buffer, and 150 μl RIPA and 1.5 μl PMSF were pipetted into each well (six-well plate). The cells in the wells were repeatedly scraped with a cell scraper after 30 min of slow shaking on ice. Heart tissue: We removed the heart specimen, cut 100 mg of myocardial tissue from the posterior wall of the left ventricle, used the homogenizer to fully disrupt the tissue, added 1 ml RIPA and 10 μl PMSF mixture into the homogenizer with the samples for each group, and slowly rotated and ground the tissue with a grinding rod. The samples were then allowed to stand on ice and ground, and the procedure was repeated for 30 min. We collected the lysate into a labeled 1.5 ml EP tube, centrifuged the tube at 12,000 tpm for 15 min in a precooled 4°C ultraspeed low-temperature centrifuge, and carefully removed the supernatant to a new labeled 1.5 ml EP tube after centrifugation, avoiding the viscous substance at the bottom of the suction tube as much as possible. The sample was then placed in a –80°C freezer for preservation. The OD value of each sample was detected using a BCA kit at a wavelength of 562 nm, and the protein concentration was calculated after plotting the standard curve. A 1/5 volume of 5×protein loading buffer was added to each sample, and the samples were dried in a bath at 100°C for 5–10 min. The samples were used after cooling and stored in a –20°C freezer.

After preparing the stacking gel and separating gel, 30 μg of protein was loaded into each lane and electrophoresed, ensuring that the sample ran straight at a constant voltage of 60 V. Following constant voltage electrophoresis at 90 V, the bromophenol blue in the sample reached the boundary between the stacking gel and the separating gel. The voltage was adjusted to 120 V, and electrophoresis was continued until the dye front reached the bottom of the gel. Following membrane transfer, the NC membrane was removed. NC membranes were cut into strips, labeled, immersed in blocking solution, blocked on a shaker at room temperature for 1 h, and then incubated overnight with rabbit anti-human CTGF (1:1000; Cell Signaling Technology), DNMT1 (1:1000;

Cell Signaling Technology), α-SMA (1:1000; Cell Signaling Technology), and collagen I (1:500; Cell Signaling Technology) and mouse anti-human β-actin (1:1000; Cell Signaling Technology) at 4°C. Then, the membranes were washed five times with TBST for more than 8 min, and HRP-conjugated goat anti-rabbit or anti-mouse IgG (1:2000) was added and incubated at room temperature for approximately 1 h. Similarly, the membrane was washed five times with TBST, and ECL chemiluminescence (Pierce) was performed with a chemiluminescence imaging system (Bio-Rad).

Bisulfite sequencing

DNA bisulfite modification and purification were performed using an EZ DNA Methylation-Direct kit (ZYMO RESEARCH, CA). The sodium bisulfite-converted DNA was amplified with TaKaRa Taq™Hot Start Version (Takara).

Statistical analysis

All experiments were performed at least in triplicate, and each experiment was independently performed at least three times. The data were analyzed using SPSS 22.0 software. The significance of differences was evaluated by the chi-square test or a two-tailed t test. Differences were considered significant at $p < 0.05$ or highly significant at $p < 0.001$. The error bars in the figures represent the SEM.

Results

Pathophysiological changes in myocardial fibrosis induced by myocardial infarction

First, post-MI myocardial fibrosis was induced in Sprague-Dawley rats, and the electrocardiogram results suggested that myocardial infarction occurred in the model mice (Fig. 1A). Echocardiography showed that the levels of left ventricular diastolic diameter (LVDd) and left ventricular systolic diameter (LVSd) were increased, while the levels of left ventricular ejection fraction (LVEF) and fractional shortening (FS) were decreased in the treated group compared with the sham group (Table 2 and Fig. 1B). HE staining showed that the cell morphology and myocardial cell arrangement were normal and collagen fibers were relatively sparse in the sham group; however, in the MI group, the myocardial cell volume was increased, the shape was irregular and disorganized, collagen fiber abundance was increased significantly, the corresponding interstitial cell numbers were also increased significantly, and fibroblast proliferation could also be seen (Fig. 1C). Then, Masson staining showed that the morphology of myocardial cells in the sham group was normal and regular, and collagen fibers were rare. However, in the MI

Table 2. Echocardiographic parameters of rats

Parameter	Sham	MI
LVSd (mm)	1.72 ± 0.13	3.32 ± 0.24*
LVDd (mm)	5.76 ± 0.29	8.23 ± 0.76*
LVEF (%)	93.45 ± 7.85	59.04 ± 6.23*
FS (%)	60.02 ± 5.25	52.13 ± 4.81*

Data are mean ± SE (n = 6 for each group), t-test, or one-way ANOVA (two-tailed). FS, fractional shortening; LVEF, left ventricular ejection fraction; LVDd, left ventricular diastolic diameter; LVSd, left ventricular systolic diameter; Sham, sham group; MI, myocardial infarction group. * $p < 0.05$ vs. MI.
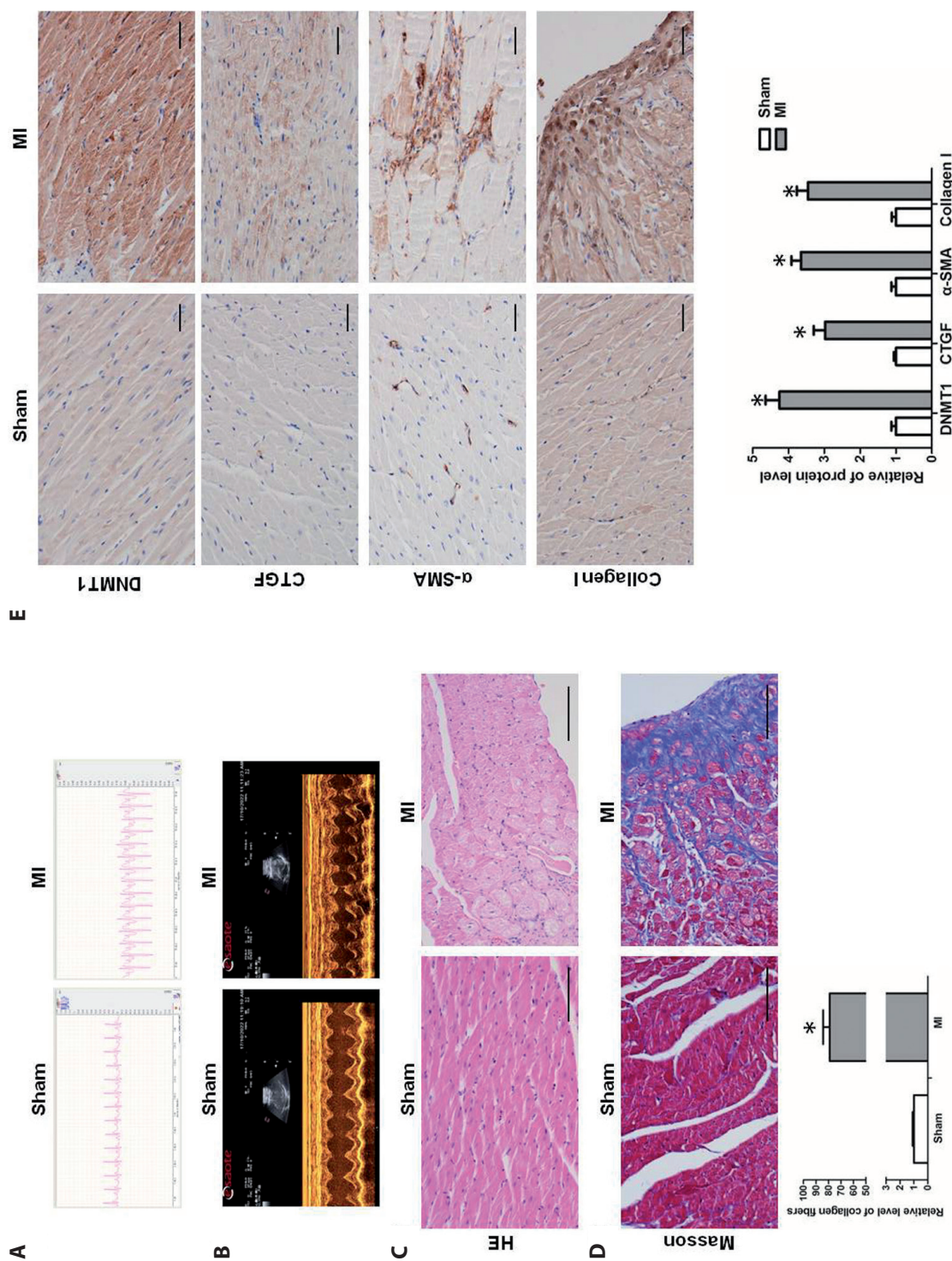
Figure 1. Pathophysiological changes of myocardial fibrosis induced by myocardial infarction. Twelve rats were randomly divided into two groups: the sham ($n = 6$) and the MI group ($n = 6$). **A.** Electrocardiogram results of rats. **B.** Echocardiographic parameters of rats. **C.** HE staining of rat ventricle samples subjected to sham and MI group. Cardiomyocytes were purplish red, and nuclei were stained blue-purple ($200\times$). **D.** Masson trichrome staining of rat ventricle samples subjected to sham and MI group. Myocardium was stained red, and collagens were stained blue ($200\times$). **E.** Immunohistochemical results of DNMT1, CTGF, a-SMA, and collagen I in myocardial tissue ($400\times$). DNMT1, DNA methyltransferase 1; a-SMA, α-smooth muscle actin; CTGF, connective tissue growth factor; MI, myocardial infarction group; Sham, sham-operated group. Scale bar = 50 μm. * $p < 0.05$

group, the myocytes were irregular in shape and arranged in a random manner, and a large number of blue-purple collagen fibers accumulated (Fig. 1D). Immunohistochemical results showed that collagen I, α-SMA, DNMT1, and CTGF expression was significantly increased in the model group compared with the sham group (Fig. 1E).

DNMT1 expression increased and miR-133b expression decreased in myocardial fibrosis

Our previous studies have confirmed that miR-133b can inhibit the activation of cardiac fibroblasts (Zhang et al. 2021). To investigate whether DNMT1 and miR-133b regulate the process of myocardial fibrosis, the expression levels of miR-133b and DNMT1 were detected in myocardial fibrosis tissues from post-MI Sprague-Dawley rats, and the results showed that DNMT1 expression increased and miR-133b expression decreased (Fig. 2A, B). A change in the degree of expression of DNMT1 and miR-133b also appeared in Ang-II-induced cardiac myofibroblasts (Fig. 2C). The above results demonstrated upregulation of TUG1 (taurine up-regulated 1) and downregulation of miR-133b and verified the phenotype in myocardial fibrosis tissues and cardiac myofibroblasts.

DNMT1 knockdown inhibited Ang-II-induced cardiac myofibroblast activation

Cardiac fibroblast activation plays a pivotal role in myocardial fibrosis. To explore the role of DNMT1 in cardiac fibrosis, we examined the expression levels of DNMT1 in Ang-II-induced cardiac fibroblasts and showed that the degree of DNMT1 expression increased after Ang-II induction (Fig. 3A). Next, we knocked down DNMT1 expression levels by transfecting TDNMT1 siRNA into cardiac fibroblasts. Knockdown of DNMT1 (Fig. 3A) counteracted the effect of Ang-II on cardiac fibroblast proliferation (Fig. 3B). In addition to proliferation, myofibroblast transformation and collagen production are key pathological features that control the

activation of cardiac fibroblasts. In cardiac fibroblast cells, the mRNA and protein levels of α-SMA, collagen I, and CTGF were upregulated following induction with Ang-II. However, knockdown of DNMT1 reversed these effects of Ang-II (Fig. 3C,D). We further explored whether DNMT1 overexpression affected cardiac fibroblast activation. Overexpression of DNMT1 in cardiac fibroblasts was induced by transfection with the DNMT1 plasmid (Fig. 3E), and overexpression of DNMT1 increased the proliferation (Fig. 3F) and collagen production (Fig. 3G,H) of cardiac myofibroblasts. These results demonstrated that DNMT1 knockdown inhibited Ang-II-induced cardiac myofibroblast activation.

DNMT1 regulated miR-133b expression via methylation during myocardial fibrosis

It is known that mRs expression can be epigenetically regulated, and previous results have revealed a negative correlation between DNMT1 expression and miR-133b levels in myocardial fibrosis tissues and cells. DNMT1 is an important methyltransferase, so we speculated that DNNT1 regulates miR-133b *via* methylation during myocardial fibrosis. In Ang-II-induced cardiac fibroblasts, DNMT1 expression levels decreased, while miR-133b expression levels increased after treatment with 5-Aza (a known inhibitor of DNA methylation) (Fig. 4A). Next, we examined the proliferation ability of cardiac fibroblasts after 5-Aza treatment, and the results showed that 5-Aza counteracted the effect of Ang-II on cardiac fibroblast proliferation (Fig. 4B). The mRNA and protein levels of α-SMA, collagen I, and CTGF were upregulated following induction with Ang-II. However, after 5-Aza treatment, these effects of Ang-II were reversed (Fig. 4C, D). Finally, BSP (Bisulfite sequencing PCR) results showed a marked decrease in methylation levels in the miR-133b promoter region upon overexpression of DNMT1, whereas knockdown of DNMT1 blocked increased methylation levels in the miR-133b promoter region in Ang-II-induced cardiac fibroblasts. Taken together, these results demonstrated that
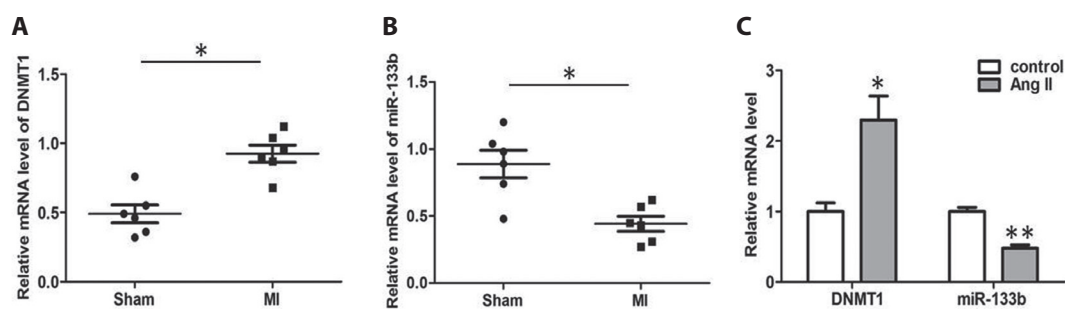

Figure 2. DNMT1 expression increased and miR-133b expression decreased in myocardial fibrosis. **A.** The expression of DNMT1 in myocardial tissue. **B.** The expression of miR-133b in myocardial tissue. **C.** The expression of DNMT11 and miR-133b in cardiac myofibroblasts induced by Ang-II. Data are mean ± SE. * $p < 0.05$. ** $p < 0.01$, *t*-test. For abbreviations, see Figure 1.
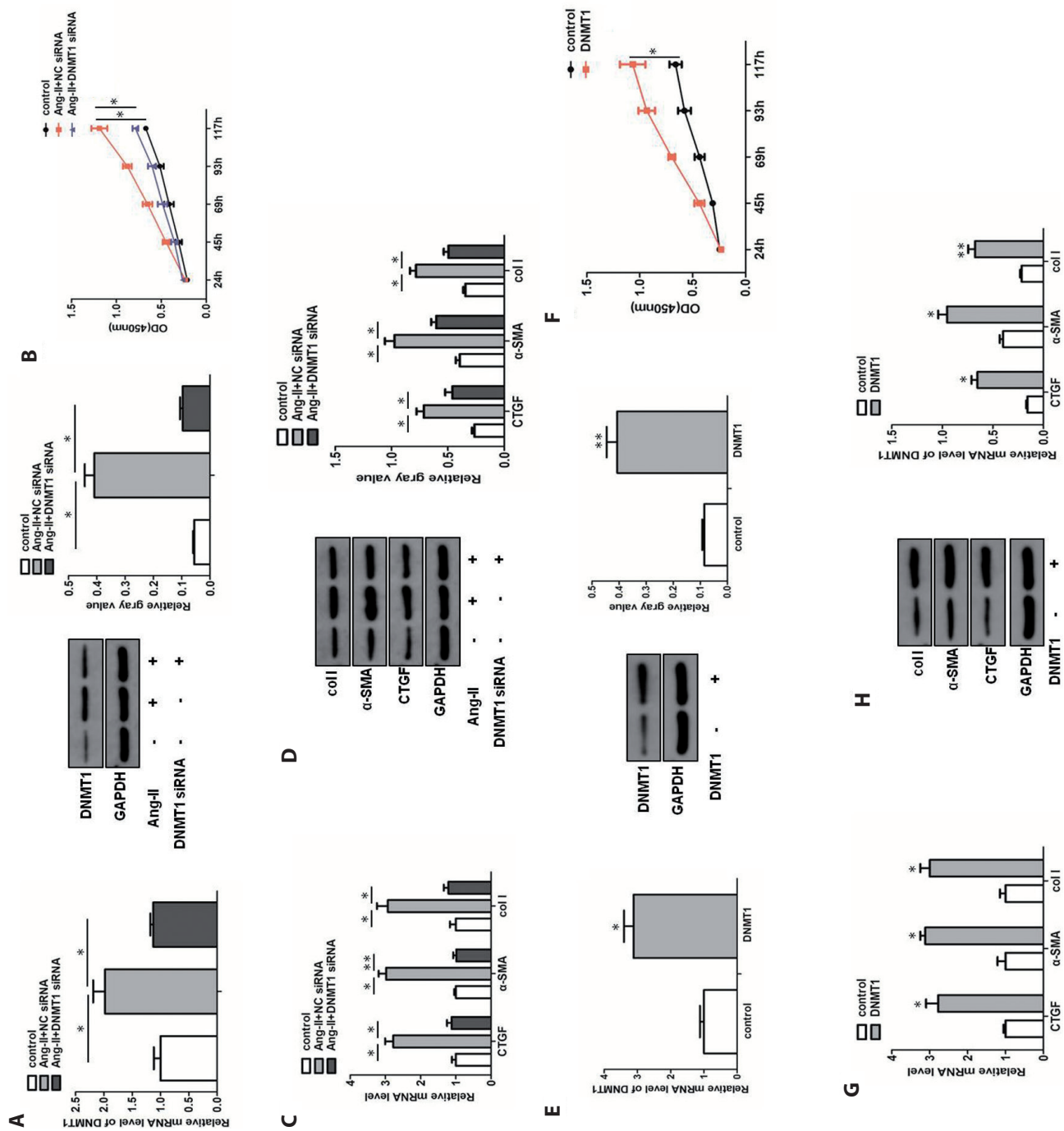
Figure 3. DNMT1 knockdown inhibited the cardiac myofibroblast activation induced by Ang-II. The activated cardiac myofibroblasts were induced with Ang-II (10 nM) for 24 h. The effect of DNMT1 siRNA on the DNMT1 expression (**A**), proliferation (**B**), mRNA expression of α-SMA, collagen I, and CTGF (**C**), and protein expression of α-SMA, collagen I, and CTGF (**D**) in Ang-II-treated cardiac myofibroblasts. The effect of pcDNA3.1-DNMT1 on the DNMT1 expression (**E**), proliferation (**F**), mRNA expression of α-SMA, collagen I, and CTGF (**G**), and protein expression of α-SMA, collagen I, and CTGF (**H**) in DNMT1-overexpression cardiac myofibroblasts. Data are mean ± SE. * $p < 0.05$. ** $p < 0.01$. col I, collagen type I. For more abbreviations, see Figure 1.
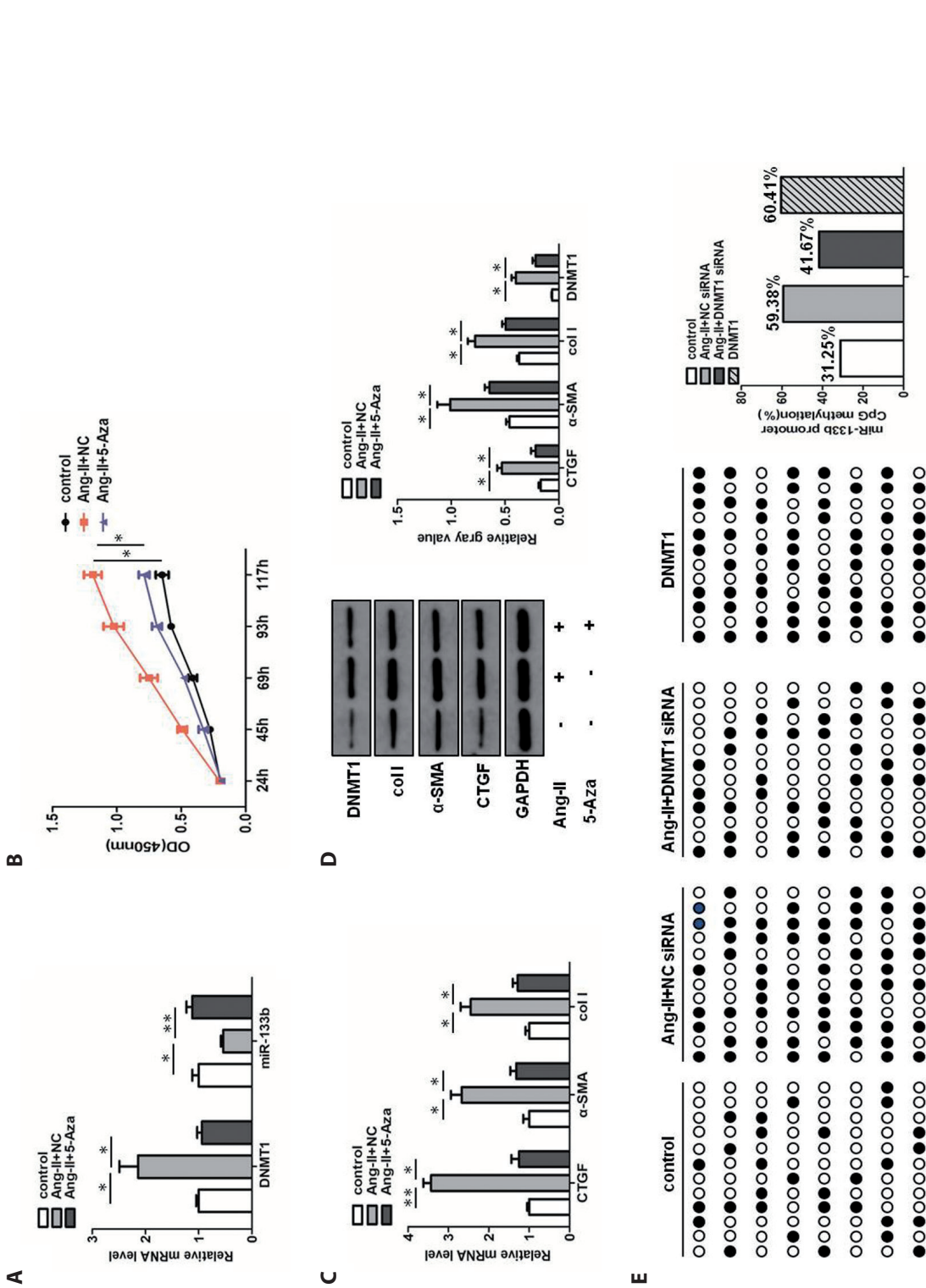
Figure 4. DNMT1 regulated miR-133b expression through methylation during myocardial fibrosis. The effect of 5-Aza (5 μM) on the DNMT1 and miR-133b expression (**A**), proliferation (**B**), mRNA expression of α-SMA, collagen I, and CTGF (**C**), and protein expression of α-SMA, collagen I, and CTGF (**D**) in Ang-II-treated cardiac myofibroblasts. **E.** Mapping of the methylation status of individual CpG sites in the miR-133b promoter by BSP assay in control, Ang-II+NC siRNA, Ang-II+DNMT1 siRNA as well as DNTM1 cells. The regions spanning the CpG island with 8 CpG sites were analyzed. Each black circle represents a methylated CpG site, while each white circle represents an unmethylated CpG site. Each row represents bisulfite sequencing of miR-133b promoter for a single analyzed random clone. Data are mean ± SE. * $p < 0.05$. ** $p < 0.01$. 5-Aza, 5-Aza-2'-deoxycytidine; BSP, Bisulfite Sequencing PCR; col I, collagen type I. For more abbreviations, see Figure 1.
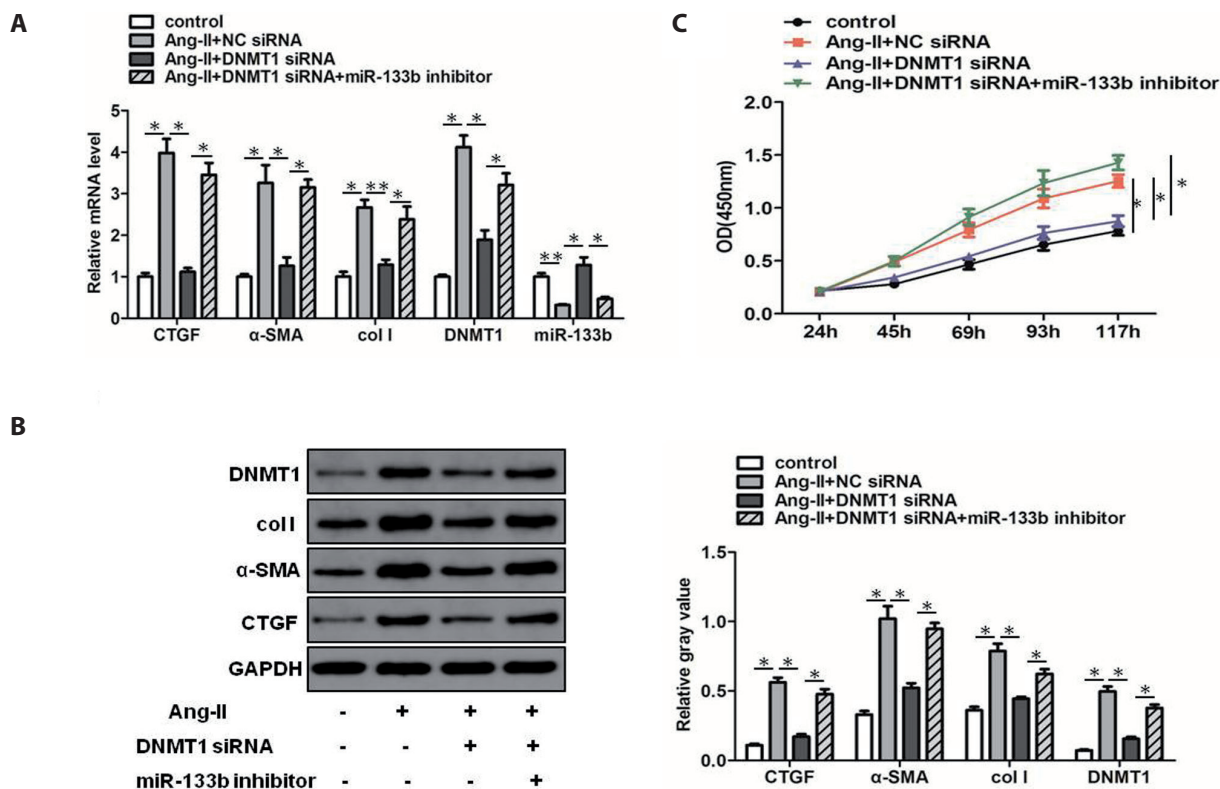
Figure 5. DNMT1 promoted cardiac myofibroblast activation through miR-133b/CTGF pathways. The effect of miR-133b inhibitor on the miR-133b, DNMT1, a-SMA, collagen I, and CTGF expression (**A, B**), and proliferation (**C**) of cardiac myofibroblasts treated with Ang-II and DNMT1 siRNA. Data are mean ± SE. * $p < 0.05$. ** $p < 0.01$. col I, collagen type I. For more abbreviations, see Figure 1.

DNMT1 regulated miR-133b expression through methylation during myocardial fibrosis.

DNMT1 promoted cardiac myofibroblast activation through the miR-133b/CTGF pathways

Next, we investigated the role of miR-133b in the DNMT1-mediated regulation of cardiac fibroblast activation, and the results showed that DNMT1 knockdown inhibited Ang II-induced cardiac fibroblast proliferation and collagen production, whereas the miR-133b inhibitor reversed the effect of knocking down DNMT1 production (Fig. 5A–C). Our previous findings have demonstrated that miR-133b can inhibit myocardial fibrosis by directly targeting CTGF (Zhang et al. 2021). Therefore, these results showed that DNMT1 promoted cardiac myofibroblast activation through the miR-133b/CTGF pathways.

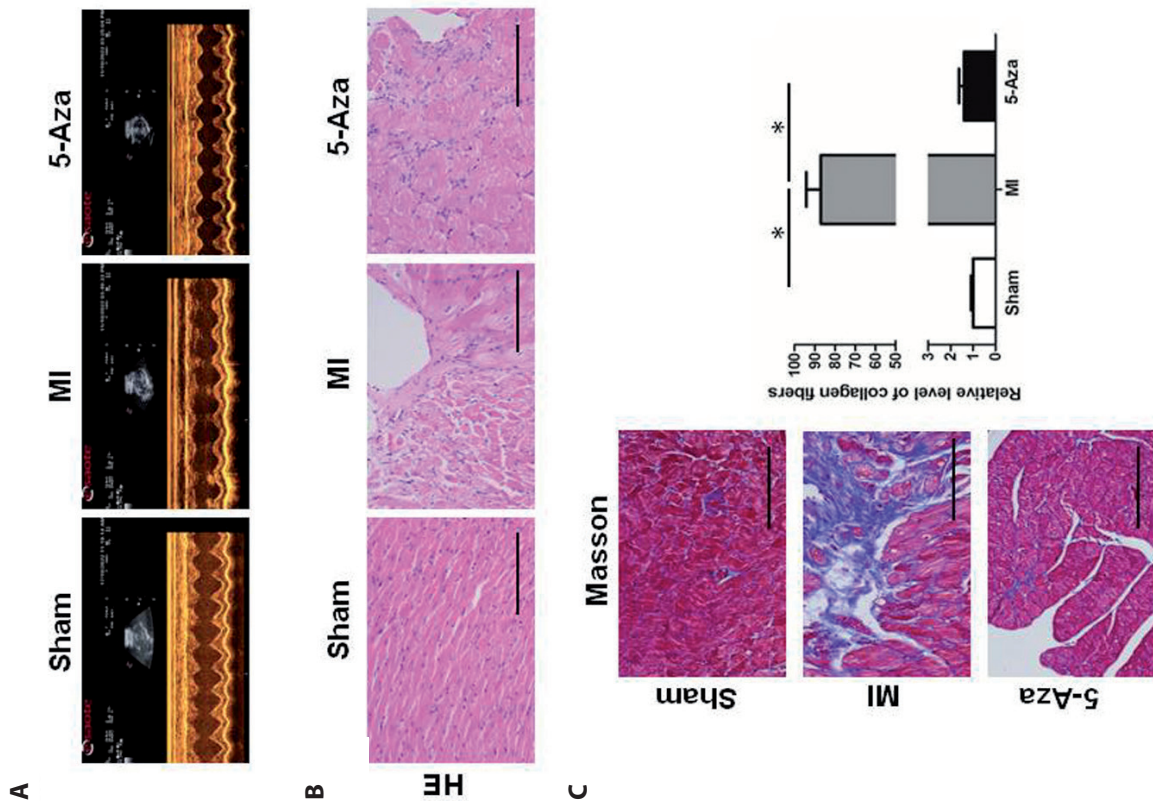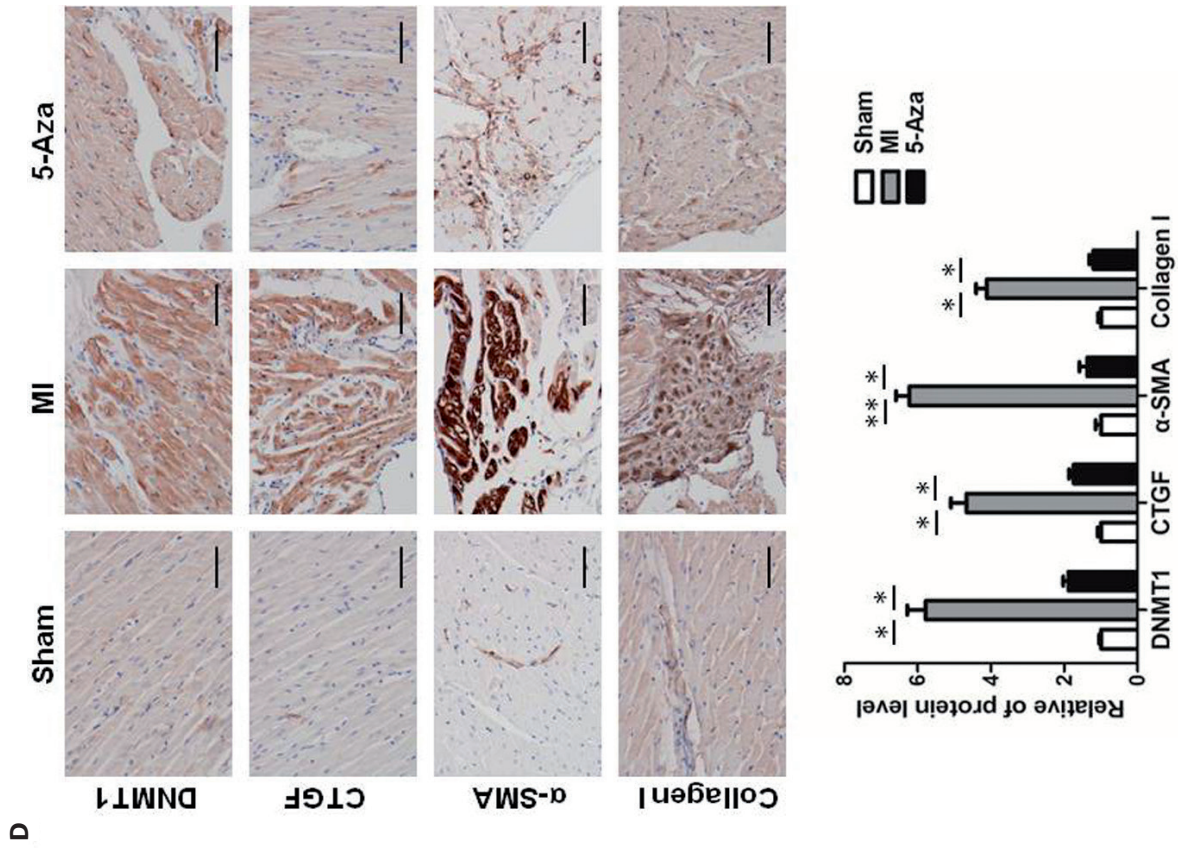### 5-Aza treatment reduced the progression of myocardial fibrosis after myocardial infarction in rats in vivo

In a rat model of myocardial fibrosis, treatment with 5-Aza resulted in decreased LVDd and LVSd values and increased LVEF and FS values by echocardiography (Fig. 6A and Table 3). HE staining showed that the size increase, irregular shape and disorganization of myocardial cells and the increased abundance of collagen fibers in MI mice were significantly improved by 5-Aza treatment (Fig. 6B). Similarly, Masson staining showed increased collagen fiber abundance in the MI group, and this change was significantly reversed after treatment with 5-Aza (Fig. 6C). Immunohistochemical results showed that collagen I, α-SMA, DNMT1, and

Table 3. Echocardiographic parameters of rats

Parameter	Sham	MI	5-Aza
LVSd (mm)	1.57 ± 0.19	3.42 ± 0.17*	2.19 ± 0.23[#]
LVDd (mm)	5.80 ± 0.48	8.33 ± 0.81*	5.71 ± 0.41[#]
LVEF (%)	91.70 ± 8.13	54.20 ± 4.78*	77.10 ± 6.17[#]
FS (%)	59.30 ± 2.19	51.50 ± 3.11*	58.30 ± 4.05[#]

Data are mean ± SE ($n = 6$ for each group), t-test, or one-way ANOVA (two-tailed). FS, fractional shortening; LVEF, left ventricular ejection fraction; LVDd, left ventricular diastolic diameter; LVSd, left ventricular systolic diameter; Sham, sham group. MI, myocardial infarction group; 5-Aza, 5-Azacytidine-treated MI group. * $p < 0.05$ *vs.* Sham; [#] $p < 0.05$ *vs.* MI.
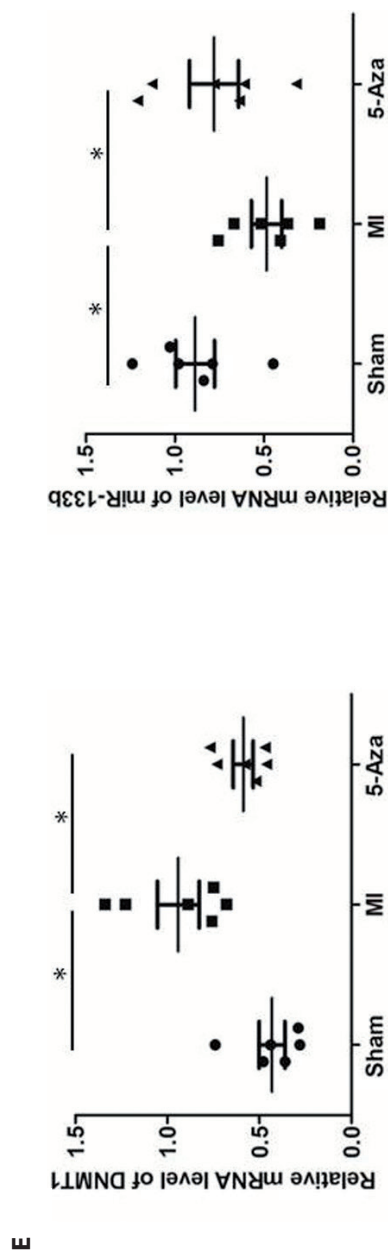
CTGF expression was significantly increased in the model group compared with the sham group, and this increase was reversed after 5-Aza treatment (Fig. 6D). In addition, we detected the expression levels of miR-133b and DNMT1 in SD rat tissues, and the results showed that DNMT1 expression increased and miR-133b expression decreased in the myocardial fibrosis model group, whereas these alterations were reversed after 5-Aza treatment (Fig. 6E). These results clarified that 5-azacytidine treatment reduced the progression of myocardial fibrosis after myocardial infarction in rats *in vivo*.

Discussion

Myocardial fibrosis is an inevitable pathological change in many end-stage heart diseases. Studies have shown that myocardial fibrosis is inseparable from the occurrence and development of myocardial remodeling and is an important pathological basis of cardiac structural remodeling (Talman and Ruskoaho 2016; Li et al. 2018). At present, the specific mechanism of myocardial fibrosis induction is not clear, but the activation and proliferation of cardiac fibroblasts has been found to be a key factor in myocardial fibrosis occurrence. Cardiac fibroblasts differentiate into myofibroblasts expressing α-smooth muscle actin (α-SMA) and secrete a variety of cytokines, and extracellular matrix proteins are very important in the development of myocardial fibrosis (Porter and Turner 2009; Tarbit et al. 2019). Collagen type I and type III are the main types of collagen in the myocardium; type I collagen is the most highly expressed, and collagen fibers are widely deposited in the extracellular matrix, eventually leading to myocardial fibrosis (Tarbit et al. 2019; Tallquist 2020). Therefore, α-SMA and collagen I are key indicators of myocardial fibrosis in laboratory tests. The mechanism of development of myocardial fibrosis is complex, and the detailed mechanism is still unclear. The present work revealed that DNMT1 expression in rats following myocardial infarction was upregulated along with myocardial fibrosis, which was also measured in cardiac fibroblasts activated under Ang-II treatment, indicating that DNMT1 plays a crucial role in myocardial fibrosis.

DNA methylation modification is an important epigenetic mechanism involved in biological processes such as gene expression regulation (Tarbit et al. 2019). DNA methylation has at least three distinct DNMTs: DNMT1, DNMT3A, and DNMT3B. DNMT1 is mainly thought to maintain hemi methylated DNA specificity and plays an important role in maintaining DNA methylation patterns during replication (Lyko 2018). Xu et al. (2015) showed that RASAL1 leads to endothelial cell mesenchymal transition (EMT) and ultimately progression of myocardial fibrosis

Figure 6. 5-Azacytidine treatment reduced the progression of myocardial fibrosis after myocardial infarction in rats *in vivo*. **A.** Echocardiographic parameters of rats. **B.** HE staining of rat ventricle samples. Cardiomyocytes were purplish red, and nuclei were stained blue-purple (200×). **C.** Masson trichrome staining of rat ventricle samples. Myocardium was stained red, and collagens were stained blue-purple (200×). **D.** Immunohistochemical results of DNMT1, CTGF, a-SMA, and collagen I in myocardial tissue (400×). **E.** The mRNA level 0f DNMT1 and miR-133b. 5-Aza, MI-operated rats were randomly assigned to receive 5- Azacytidine at a dose of 5 mg/kg or control (DMSO-PBS) *via* intraperitoneal injection (*n* = 6 *per* group). Scale bar = 50 μm. For more abbreviations, see Figure 1.

through aberrant promoter methylation. Methylation of CpG island promoters is a typical epigenetic mechanism that stably controls gene expression. The aim of this study was to elucidate the contribution of aberrant promoter DNA methylation to pathological EMT and subsequent myocardial fibrosis (Xu et al. 2015). Tao et al. (2014) showed that silencing of RASSF1A by DNMT3A promotes cardiac fibrosis through upregulation of ERK1/2. Tan et al. (2016) demonstrated that human coronary artery endothelial cells (HCAECs) undergo endothelial cell mesenchymal transition when exposed to excessive phosphate levels, further demonstrating that EMT is initiated by abnormal phosphorylated DNMT1 recruitment to the RASAL1 CpG island promoter of HDAC2, causing abnormal promoter methylation and transcriptional repression; this ultimately leads to increased Ras-GTP activity and EMT development, thereby promoting fibroblast proliferation and subsequent development of myocardial fibrosis. Collectively, these findings support the importance of the role of DNA methylation in the pathogenesis and progression of myocardial fibrosis, underscoring the potentially favorable impact of DNA methylation inhibitors in the prevention and treatment of this degenerative heart disease. In our study, we showed that DNMT1 knockdown promoted miR-133b expression, and in addition, DNMT1 expression levels decreased, whereas miR-133b expression levels increased after 5-Aza-treatment in Ang-II-induced cardiac fibroblasts. BSP results showed that the methylation levels of the miR-133b promoter region were significantly decreased after overexpression of DNMT1, while knockdown of DNMT1 blocked the Ang-II-induced increase in the methylation levels of the miR-133b promoter region in cardiac fibroblasts. To date, a relationship between DNMT1 and miR-133b has not been reported.

miRs are a series of small noncoding RNAs with a length of approximately 22 bases that are involved in the regulation of posttranscriptional gene expression and are upstream mediators of multitarget and multigene regulation (Gierlikowski and Gierlikowska 2022). They have complex and very flexible regulatory mechanisms, and their target proteins and biological pathways are involved in many different cell types and tissues (Mohr and Mott 2015; Lu and Rothenberg 2018). Numerous studies have shown that microRNAs play an important role in almost all cellular homeostasis processes, and loss of their regulation leads to the development of a range of diseases (Lu and Rothenberg 2018). Pathologic changes in the heart have been reported to be associated with alterations in gene expression. It has been shown that multiple miRNAs (e.g., miR-133a (Liu et al. 2022), miR-503 (Zhou et al. 2016), miR-101 (Zhao et al. 2015), and miR-2 (Adam et al. 2015)) have been demonstrated to influence the physiological function of cardiac myofibroblasts and thus exert antifibrotic effects. In the present study, miR-133b was observed to be downregulated

in Ang II-induced activated cardiac fibroblasts and inhibited by DNMT1 knockdown or 5-Aza treatment. Downregulation of miR-133b expression by a miR-133b inhibitor caused increased proliferation and collagen production in cardiac fibroblasts. These results demonstrated that inhibition of miR-133b could reverse the effect of DNMT1 knockdown on cardiac fibroblast activation.

CTGF, also known as CNN2, acts as a downstream molecule of TGF-β, and CTGF plays a critical role in myocardial fibrosis (Hong et al. 2018). When myocardial fibrosis developed, the expression level of CTGF was significantly upregulated. In our previous study, CTGF was found to be a target of miR-133b, and miR-133b knockdown suppressed myocardial fibrosis activation by directly targeting CTGF (Zhang et al. 2021). Thus, the results of this study confirmed that DNMT1 promotes myocardial fibrosis through the miR-133b/CTGF pathway.

Conclusion

Our study suggests that DNMT1 mediates CTGF expression during cardiac fibroblast activation by regulating the methylation of miR-133b. The present work reveals the unique role of the DNMT1/miR-133b/CTGF axis in myocardial fibrosis, thus suggesting its great therapeutic potential in the treatment of cardiac diseases.

References

Adam O, Zimmer C, Hanke N, Hartmann RW, Klemmer B, Böhm M, Laufs U (2015): Inhibition of aldosterone synthase (CYP11B2) by torasemide prevents atrial fibrosis and atrial fibrillation in mice. J. Mol. Cell Cardiol. **85,** 140-150
https://doi.org/10.1016/j.yjmcc.2015.05.019

Brulport A, Vaiman D, Chagnon MC, Le Corre L (2020): Obesogen effect of bisphenol S alters mRNA expression and DNA methylation profiling in male mouse liver. Chemosphere **241,** 125092
https://doi.org/10.1016/j.chemosphere.2019.125092

Frangogiannis NG (2021): Cardiac fibrosis. Cardiovasc. Res. **117,** 1450-1488
https://doi.org/10.1093/cvr/cvaa324

Gierlikowski W, Gierlikowska B (2022): MicroRNAs as regulators of phagocytosis. Cells **11,** 1380

https://doi.org/10.3390/cells11091380

González A, Schelbert EB, Díez J, Butler J (2018): Myocardial interstitial fibrosis in heart failure: Biological and translational perspectives. J. Am. Coll. Cardiol. **71,** 1696-1706
https://doi.org/10.1016/j.jacc.2018.02.021

Hong L, Lai HL, Fang Y, Tao Y, Qiu Y (2018): Silencing CTGF/CCN2 inactivates the MAPK signaling pathway to alleviate myocardial fibrosis and left ventricular hypertrophy in rats with dilated cardiomyopathy. J. Cell. Biochem. **119,** 9519-9531
https://doi.org/10.1002/jcb.27268

Kurose H (2021): Cardiac fibrosis and fibroblasts. Cells **10,** 1716
https://doi.org/10.3390/cells10071716

Laggerbauer B, Engelhardt S (2022): MicroRNAs as therapeutic targets in cardiovascular disease. J. Clin. Invest. **132,** e159179
https://doi.org/10.1172/JCI159179

Li L, Zhao Q, Kong W (2018): Extracellular matrix remodeling and cardiac fibrosis. Matrix Biol. **68-69,** 490-506
https://doi.org/10.1016/j.matbio.2018.01.013

Li X, Yang Y, Chen S, Zhou J, Li J, Cheng Y (2021): Epigenetics-based therapeutics for myocardial fibrosis. Life Sci. **271,** 119186
https://doi.org/10.1016/j.lfs.2021.119186

Liu M, López de Juan Abad B, Cheng K (2021): Cardiac fibrosis: Myofibroblast-mediated pathological regulation and drug delivery strategies. Adv. Drug Deliv. Rev. **173,** 504-519
https://doi.org/10.1016/j.addr.2021.03.021

Liu N, Xie L, Xiao P, Chen X, Kong W, Lou Q, Lu X (2022): Cardiac fibroblasts secrete exosome microRNA to suppress cardiomyocyte pyroptosis in myocardial ischemia/reperfusion injury. Mol. Cell Biochem. **477,** 1249-1260
https://doi.org/10.1007/s11010-021-04343-7

Long F, Wang Q, Yang D, Zhu M, Wang J, Zhu Y, Liu X (2020): Targeting JMJD3 histone demethylase mediates cardiac fibrosis and cardiac function following myocardial infarction. Biochem. Biophys. Res. Commun. **528,** 671-677
https://doi.org/10.1016/j.bbrc.2020.05.115

Lu TX, Rothenberg ME (2018): MicroRNA. J. Allergy Clin. Immunol. **141,** 1202-1207
https://doi.org/10.1016/j.jaci.2017.08.034

Lyko F (2018): The DNA methyltransferase family: a versatile toolkit for epigenetic regulation. Nat. Rev. Genet. **19,** 81-92
https://doi.org/10.1038/nrg.2017.80

Mohr AM, Mott JL (2015): Overview of microRNA biology. Semin. Liver Dis. **35,** 3-11
https://doi.org/10.1055/s-0034-1397344

Porter KE, Turner NA (2009): Cardiac fibroblasts: at the heart of myocardial remodeling. Pharmacol. Ther. **123,** 255-278
https://doi.org/10.1016/j.pharmthera.2009.05.002

Saliminejad K, Khorram Khorshid HR, Soleymani Fard S, Ghaffari SH (2019): An overview of microRNAs: Biology functions therapeutics and analysis methods. J. Cell. Physiol. **234,** 5451-5465
https://doi.org/10.1002/jcp.27486

Tallquist MD (2020): Cardiac fibroblast diversity. Annu Rev. Physiol. **82,** 63-78
https://doi.org/10.1146/annurev-physiol-021119-034527

Talman V, Ruskoaho H (2016): Cardiac fibrosis in myocardial infarction-from repair and remodeling to regeneration. Cell Tissue Res. **365,** 563-581
https://doi.org/10.1007/s00441-016-2431-9

Tan X, Xu X, Zeisberg M, Zeisberg EM (2016): DNMT1 and HDAC2 cooperate to facilitate aberrant promoter methylation in inorganic phosphate-induced endothelial-mesenchymal transition. PLoS One **11,** e0147816
https://doi.org/10.1371/journal.pone.0147816

Tao H, Yang JJ, Shi KH, Deng ZY, Li J (2014): DNA methylation in cardiac fibrosis: new advances and perspectives. Toxicology **323,** 125-129
https://doi.org/10.1016/j.tox.2014.07.002

Tarbit E, Singh I, Peart JN, Rose'Meyer RB (2019): Biomarkers for the identification of cardiac fibroblast and myofibroblast cells. Heart Fail. Rev. **24,** 1-15
https://doi.org/10.1007/s10741-018-9720-1

Wojciechowska A, Braniewska A, Kozar-Kamińska K (2017): MicroRNA in cardiovascular biology and disease. Adv. Clin. Exp. Med. **26,** 865-874
https://doi.org/10.17219/acem/62915

Xu X, Tan X, Tampe B, Nyamsuren G, Liu X, Maier LS, Zeisberg EM (2015): Epigenetic balance of aberrant Rasal1 promoter methylation and hydroxymethylation regulates cardiac fibrosis. Cardiovasc. Res. **105,** 279-291
https://doi.org/10.1093/cvr/cvv015

Yang JJ, She Q, Yang Y, Tao H, Li J (2018): DNMT1 controls LncRNA H19/ERK signal pathway in hepatic stellate cell activation and fibrosis. Toxicol. Lett. **295,** 325-334
https://doi.org/10.1016/j.toxlet.2018.07.013

Zhang S, Wang N, Ma Q, Fan F, Ma X (2021): LncRNA TUG1 acts as a competing endogenous RNA to mediate CTGF expression by sponging miR-133b in myocardial fibrosis after myocardial infarction. Cell. Biol. Int. **45,** 2534-2543
https://doi.org/10.1002/cbin.11707

Zhao X, Wang K, Hu F, Qian C, Guan H, Feng K, Chen Z (2015): MicroRNA-101 protects cardiac fibroblasts from hypoxia-induced apoptosis via inhibition of the TGF-β signaling pathway. Int. J. Biochem. Cell Biol. **65,** 155-164
https://doi.org/10.1016/j.biocel.2015.06.005

Zhao Y, Qin F, Han S, Li S, Wang H, Tian J, Cen X (2022): MicroRNAs in drug addiction: Current status and future perspectives. Pharmacol. Ther. **236,** 108215
https://doi.org/10.1016/j.pharmthera.2022.108215

Zhou Y, Deng L, Zhao D, Chen L, Yao Z, Guo X, Shan H (2016): MicroRNA-503 promotes angiotensin II-induced cardiac fibrosis by targeting Apelin-13. J. Cell. Mol. Med. **20,** 495-505
https://doi.org/10.1111/jcmm.12754

Zhu H, He C, Zhao H, Jiang W, Xu S, Li J, Huang C (2020): Sennoside A prevents liver fibrosis by binding DNMT1 and suppressing DNMT1-mediated PTEN hypermethylation in HSC activation and proliferation. FASEB J. **34,** 14558-14571
https://doi.org/10.1096/fj.202000494RR